European Heart Journal - Cardiovascular Imaging (2017) **18**, 510–518
doi:10.1093/ehjci/jew228

Everolimus-eluting stents stabilize plaque inflammation *in vivo*: assessment by intravascular fluorescence molecular imaging

Marcella A. Calfon Press[1,2], Georgios Mallas[1,3], Amir Rosenthal[1,4], Tetsuya Hara[1], Adam Mauskapf[1], R. Nika Nudelman[4], Alexander Sheehy[5], Igor V. Polyakov[5], Frank Kolodgie[6], Renu Virmani[6], J. Luis Guerrero[1], Vasilis Ntziachristos[4], and Farouc A. Jaffer[1,7]*

[1]Cardiology Division, Cardiovascular Research Center, Massachusetts General Hospital, Harvard Medical School, Simches Research Building Room 3206, 185 Cambridge Street, Boston, MA 02114, USA; [2]Department of Cardiology, Ronald Reagan Medical Center, University of California in Los Angeles, Los Angeles CA, USA; [3]Department of Electrical and Computer Engineering, Northeastern University, Boston, MA, USA; [4]Institute for Biological and Medical Imaging (IBMI), Helmholtz Center Munich & Technical University of Munich, Munich, Germany; [5]Abbott Vascular Laboratories, Santa Clara, CA, USA; [6]CV Path Institute, Gaithersburg, MD, USA; and [7]Center for Molecular Imaging Research, Massachusetts General Hospital, Harvard Medical School, Boston, MA, USA

Received 8 April 2016; accepted after revision 2 October 2016; online publish-ahead-of-print 30 December 2016

Aims Inflammation drives atherosclerosis complications and is a promising therapeutic target for plaque stabilization. At present, it is unknown whether local stenting approaches can stabilize plaque inflammation *in vivo*. Here, we investigate whether everolimus-eluting stents (EES) can locally suppress plaque inflammatory protease activity *in vivo* using intravascular near-infrared fluorescence (NIRF) molecular imaging.

Methods and results Balloon-injured, hyperlipidaemic rabbits with atherosclerosis received non-overlapping EES and bare metal stents (BMS) placement into the infrarenal aorta ($n = 7$ EES, $n = 7$ BMS, 3.5 mm diameter x 12 mm length). Four weeks later, rabbits received an injection of the cysteine protease-activatable NIRF imaging agent Prosense VM110. Twenty-four hours later, co-registered intravascular 2D NIRF, X-ray angiography and intravascular ultrasound imaging were performed. *In vivo* EES-stented plaques contained substantially reduced NIRF inflammatory protease activity compared with untreated plaques and BMS-stented plaques ($P = 0.006$). *Ex vivo* macroscopic NIRF imaging of plaque protease activity corroborated the *in vivo* results ($P = 0.003$). Histopathology analyses revealed that EES-treated plaques showed reduced neointimal and medial arterial macrophage and cathepsin B expression compared with unstented and BMS-treated plaques.

Conclusions EES-stenting stabilizes plaque inflammation as assessed by translational intravascular NIRF molecular imaging *in vivo*. These data further support that EES may provide a local approach for stabilizing inflamed plaques.

Keywords atherosclerosis • inflammation • stent • everolimus • fluorescence imaging • molecular imaging

Introduction

Inflammation is a major driver of plaque complications. Substantial experimental evidence demonstrates that inflammatory macrophages and augmented protease activity mediate the initiation, progression, and complication of high-risk plaques.[1] Clinical studies further demonstrate the importance of inflammation in predicting adverse cardiovascular outcomes.[2] Inflammation therefore represents an attractive therapeutic target in atherosclerosis, as currently being tested by systemic anti-inflammatory therapies such as methotrexate and canakinumab.[1]

With the long-term goal of reducing coronary events, pre-emptive stenting of high-risk coronary plaques has been preliminary

* Corresponding author. Tel: +1 617 724 9353; Fax: +1 617 860 3180. E-mail: fjaffer@mgh.harvard.edu

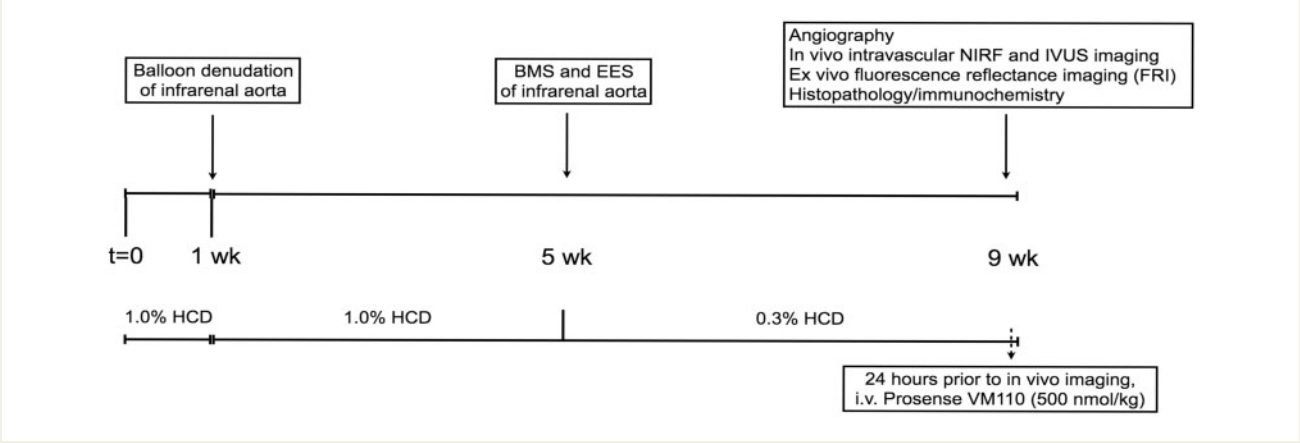

Figure 1 Schema of the experimental protocol assessing the effects of EES and BMS on inflammatory atherosclerosis in the aorta of New Zealand white rabbits. IVUS, intravascular ultrasound; BMS, bare metal stent; EES, everolimus-eluting stent; NIRF, near-infrared fluorescence.

investigated human subjects.[3] In addition, drug-eluting stents, including everolimus-eluting stents (EES), have been shown to reduce macrophage content experimentally,[4–6] and therefore may be attractive for treating inflamed plaques.

At present, the ability of the DES to stabilize plaque inflammation, and specifically plaque protease activity *in vivo*, remains unknown. Here, we utilize intravascular near-infrared fluorescence (NIRF) molecular imaging to investigate the inflammation-stabilizing effects of EES implanted into atheroma of rabbit arteries. Intravascular NIRF imaging is a new, translatable approach to image plaque biology in coronary-sized arteries *in vivo*.[7,8] In this experimental study, we apply intravascular NIRF molecular imaging to assess the ability of EES to reduce *in vivo* cysteine protease activity, an important macrophage-derived mediator of plaque destabilization,[9,10] and compare these effects with BMS and unstented segments.

Methods

Animal studies

The Subcommittee on Research Animal Care at Massachusetts General Hospital approved all animal studies. A balloon injury, hyperlipidaemic protocol was used to generate inflamed aortic atheroma with elevated cysteine protease activity.[8] New Zealand white rabbits ($n = 7$, 3.0–3.5 kg, Millbrook Farms, Amherst, MA, USA) were fed a hypercholesterolaemic diet (1% cholesterol and 5% peanut oil, C-30293, Research Diets, Inc., New Brunswick, NJ, USA) for 1 week prior to aortic balloon injury (*Figure 1*). After an overnight fast, animals were anesthetized with intramuscular ketamine (35 mg/kg) and inhaled isoflurane (1–5% vol/vol, Baxter, Deerfield, IL, USA). A 5F introducer was inserted into the left iliac artery using fluoroscopic guidance. Intra-arterial heparin (150 units/kg) and nitroglycerin (50–100 μg) were administered. A baseline angiogram using an intra-arterial injection of iodinated contrast agent (Ultravist, Bayer HealthCare) was then performed. Next, a 3F Fogarty arterial embolectomy catheter (Edwards Lifesciences, Irvine, CA, USA) was advanced into the abdominal aorta. The balloon was inflated to tension (0.5-1 cc, air) and three pullbacks along vessel were performed from the renal arteries to the iliac bifurcation. Following denudation, the catheter was removed and the left iliac artery was ligated. Animals were then continued on 1% high-cholesterol diet for four more weeks.

At Day 28 after initial balloon injury and after an overnight fast, animals were anesthetized with intramuscular ketamine and inhaled isoflurane. A 5F introducer was inserted into the left carotid artery using fluoroscopic guidance. A 0.014″ guidewire was next introduced into the abdominal aorta and distally positioned within the right iliac artery. To guide deployment of stents into areas of plaque along the injured aorta, an intravascular ultrasound catheter (Boston Scientific Corporation, Natick, MA) was inserted over the 0.014″ guidewire and a pullback was performed across the entire length of the aorta from the iliac bifurcation to the renal arteries. Under fluoroscopic and IVUS guidance, aortic plaques were then stented with a non-overlapping bare metal stent (BMS, ML VISION, 3.5 mm diameter x 12 mm length, 9 atm deployment pressure, Abbott Vascular, CA) and an EES (XIENCE V, 3.5 mm x 12 mm, 9 atm deployment pressure). The orientation of BMS and DES in the proximal and distal segments of the abdominal aorta was randomly reversed. After stenting, animals were changed to 0.3% cholesterol diet (C-30255, Research Diets, Inc.) that was continued for additional 4 weeks (total 8 weeks post-balloon denudation, *Figure 1*).

2D intravascular NIRF imaging system

Intravascular NIRF imaging studies employed a standalone rotational 2D NIRF imaging apparatus and catheter that was recently established for intravascular NIRF molecular imaging.[7,11] Briefly, the NIRF catheter consists of an optical fibre (100/140 μm core/clad diameter) that illuminates the vessel wall using a 750-nm laser excitation source. Laser light of power approximately equal to 15 mW is emitted at a 90° angle relative to fibre axis. Subsequent fluorescent light is collected by the same fibre and guided to a detection system that includes optical filters to reject back-scattered laser light and a photomultiplier tube for low-light detection. A radio-opaque ferrule is mounted on the tip of the fibre and a polyethylene tubing with a 2.9-French (0.965 mm) outer diameter is used for housing. The imaging system utilizes two automated motors (rotational and translational) to enable concomitant 360° imaging and longitudinal pullback to obtain true 2D imaging (angular and longitudinal readouts).

NIRF molecular imaging of cysteine protease activity

To image cathepsin cysteine protease activity *in vivo*, we utilized a NIRF agent consisting of a poly-lysine polymer backbone derivatized with multiple NIR fluorophores (Prosense VM110 (VM110), ex/em 750/780 nm, PerkinElmer, Waltham, MA, USA). Close proximity of NIR fluorophores produces intramolecular quenching at baseline.[7] Following targeted enzymatic cleavage by cysteine proteases such as cathepsin B, the fluorophores separate, resulting in substantial amplification of the NIRF signal. Cathepsin B is a robust biomarker of Prosense VM110 activation in atherosclerosis.[7,8,12]

Intravascular multimodal imaging of EES and BMS effects on plaque inflammation

Eight weeks following balloon injury and 4 weeks after aortic stenting, rabbits received an intravenous injection of the cysteine protease activatable NIRF imaging agent Prosense VM110 at a dose of 500 nmol/kg.[7] Twenty-four hours later, angiography and IVUS were performed as described above, followed by multiple automated NIRF catheter pullbacks spanning the length of the implanted aortic stents. From a series of co-registered pullbacks, the pullback with the highest NIRF signal (and therefore presumably lowest blood attenuation) was used for *in vivo* analyses. The NIRF catheter was advanced over a 0.014″ guidewire using a standard monorail system. The distal tip of the NIRF catheter was advanced into the iliac artery and three to four serial 100 mm pullbacks were performed (rotational speed 30–100 rpm). NIRF imaging was performed through blood without flushing, as previously described.[7] IVUS was performed thereafter to assess plaque and stent architecture.

Intravascular 2D NIRF image analyses

Target-to-background ratios (TBRs) were calculated using MATLAB 7.10.0 (R2010a, MathWorks, Natick, MA, USA). The data were filtered with an appropriate low-pass finite impulse response (FIR) filter to remove the high-frequency electronic noise. To remove low frequency laser-induced fluctuations, the data were then passed through a high pass FIR filter. The IVUS pullback of each animal was used to anatomically define four regions-of-interest (ROIs): a normal region (no intimal thickening), an unstented plaque region, the EES region, and the BMS region. The mean signal across each region was calculated and the mean signal of the normal region was defined as the background. Next, the TBR of each region was calculated as the ratio of the mean signal of the target region divided by the mean signal of the background. Normal regions were identified as zones that did not undergo balloon denudation or stenting (i.e. either sections of iliac artery or distal aorta) during X-ray visualization. The absence of plaque within these zones was confirmed using IVUS and again by direct *ex vivo* visualization after dissection where areas of plaque could easily be distinguished from plaque-free zones. Previous studies with this rabbit model demonstrate that uninjured segments develop minimal atheroma.[7,8]

Intravascular NIRF-IVUS alignment and fusion

The NIRF and IVUS datasets were first aligned in the longitudinal axis based on the start of the pullback position on X-ray, which was determined using the radiopaque catheter tips present on both NIRF and IVUS catheters.[7] X-ray and IVUS images were co-registered based on the anatomical landmarks of the iliac bifurcation, implanted stents, and renal arteries. Rotational co-registration of NIRF and IVUS images was not performed, as it was not possible to guarantee that the rotational position of the separate NIRF and IVUS catheters would remain fixed throughout the pullbacks.

The NIRF data were fused with the IVUS longview pullbacks (MATLAB). Initially, the NIRF data were filtered as described above and then smoothed with a Gaussian filter. Next a 1D profile was calculated for the NIRF pullback by averaging the signal over all angles for each pullback position. After aligning the IVUS longview with the NIRF pullback, the amplitude of the NIRF 1D profile was presented using a 'hot' colourmap.[7]

Ex vivo fluorescence reflectance imaging

After imaging and sacrifice, aortoiliac vessels were surgically resected and then elongated to lengths measured on the *in vivo* angiogram and IVUS datasets. Fluorescence reflectance imaging (FRI) was performed at multiple wavelengths using a commercially available FRI system (Olympus Small Animal Imaging System OV110, Olympus, Tokyo, Japan) equipped with multichannel filters (Omega Optical, Brattleboro, VT, USA): bandpass excitation 716–756 nm, bandpass emission 780–820 nm. A series of exposure times were utilized for each wavelength (0.5, 1, 2.5 and 5 s) and acquired images were exported as DICOM files for further analyses. As controls, the liver, spleen, kidney, and heart were imaged at similar channels and exposure times. Using white light and 535 nm excitation autofluorescence images, plaques, stented zones, and normal areas were identified for NIRF TBR analyses. ROIs were manually traced on FRI images using visual identification of normal vessel, plaque, and stented zones (Osirix version 2.7.5, Pixmeo, Switzerland). For stented zones, an ROI was traced around each visible stent (total length of ROI drawn was 12 mm per DES and per BMS), as well as in 3 mm intervals across the stent and flanking stent edges. For plaque TBR calculation, an ROI was manually drawn around plaques that were imaged *in vivo*; the average TBR from these zones were reported. The background normal vessel ROI was selected from the white light and autofluorescence images. The TBR was calculated as the average target signal divided by the average background signal (normal vessel).

Histopathology

Tissue preparation

Tissue from four animals was submitted for histopathology. The aorta from each animal contained two stents (EES and BMS), for a total of four EES and four BMS that underwent histopathological analysis. Stented tissue was fixed in formalin and shipped on dry ice to CVPath (Gaithersburg, MD, USA) for processing and analyses. Sections were examined by light microscopy for the presence of inflammation, thrombus, neointimal formation, and vessel wall injury. The stents were segmented at 5–6 mm-intervals in cross-section using tungsten-carbide scissors with a serrated edge. In select segments for cryosectioning, the stent wires were carefully cut and pulled with intent not to destroy the tissue architecture. Adjacent sections were kept intact and submitted for resin embedding.

Resin embedding

Stented vessel segments were dehydrated in a graded series of ethanol and embedded in methylmethacrylate (MMA) plastic. Sections from the proximal, middle, and distal region of the stent were then cut on a rotary microtome at 4–6 μm, mounted on glass slides and stained as above. Additional sections were held in reserve for IHC.

Cryosectioning

Owing to limitations in immunohistochemical staining for cathepsin B on resin-embedded samples, a single stented vessel from each study arm was preserved for immunohistochemical staining from cryosections. Prior to cryosectioning, the stented tissue was snap-frozen in optimal cutting temperature tissue processing medium (Miles Diagnostics, Elkhart, IN, USA). Serial cryostat sections (proximal, middle, and distal) (6 μm) were then cut and air-dried onto Superfrost microslides and stained by haematoxylin and eosin (H&E) and Movat's Pentachrome. Adjacent sections were held in reserve at −70 °C for subsequent immunohistochemistry (IHC).

Morphometry

Resin embedded section analysis was accomplished using a NIST calibrated microscope system (IP Lab software, Rockville, MD, USA). The cross-sectional areas [external elastic lamina (EEL), internal elastic lamina (IEL), stent area, and lumen] of each stented section were measured. Neointimal thickness was measured as the distance from the inner surface of each stent strut to the luminal border. Area measurements were used to calculate vessel layer areas with the following formulas:

$$\text{Media} = \text{EEL} - \text{IEL}.$$

$$\text{Neointima} = \text{IEL} - \text{lumen}.$$

$$\%\ \text{Stenosis} = [1 - (\text{Lumen Area}/\text{IEL Area})] \times 100$$

IHC

Serial sections were immunostained with antibodies for the macrophage marker RAM-11 (resin-embedded, $n = 4$ vessels, dilution 1:200, Dako; cryosectioned, $n = 1$ stent, Dako) and the protease cathepsin B (cryostat, $n = 1$ vessels, dilution 1:20, sc-6493, Santa Cruz) with exposure of 60 or 120 min, respectively. The primary antibodies were then labelled with a biotinylated link antibody directed against mouse antigen with the use of a peroxidase-base (LSAB, Dako) and visualized by 3-amino-9-ethylcarbozle substrate; the sections were subsequently counterstained with Gill's hematoxylin (Sigma-Aldrich). Omission of a primary antibody served as a specificity control (data not shown). Computer-assisted colour image analysis segmentation with background correction was used to quantify IHC staining of RAM-11 positive macrophages. The percentage of positive RAM-11 staining was expressed as a function of total plaque area.

Statistical analyses

For all comparisons of TBR and mean signals between unstented, BMS, EES, and plaque areas of interest, the median with inter-quartile range (IQR) were calculated using Prism (Version 5.0c, GraphPad, La Jolla, CA, USA). For stented zones, an ROI was traced around each visible stent (total length of ROI drawn was 12 mm per DES and per BMS), as well as around 3 mm intervals across the stent and flanking stent edges. Statistically significant differences among groups were determined using the Kruskal–Wallis test for non-parametric distributions. Dunn's multiple comparison test was used to compare differences between groups. Statistical differences of macrophage expression among groups were assessed using the Kruskal–Wallis test for non-parametric distributions followed by Dunn's multiple comparison test to compare differences between groups. For morphometric comparisons of % stenosis and neointimal area between BMS and EES, the Mann–Whitney test was applied. A value of $P < 0.05$ was considered statistically significant.

Results

Everolimus-eluting DES locally suppresses plaque cysteine protease activity *in vivo*, as detected by intravascular NIRF molecular imaging

EES have the potential to stabilize inflamed plaques *in vivo*. To detect the effects of EES on plaque inflammation *in vivo*, NIRF cathepsin inflammatory protease activity was detected via a 2.9F intravascular imaging catheter that allowed 2D spatial mapping of NIR fluorescence signals through blood in coronary-sized arteries.[7] Four weeks after rabbits with aortic atheroma were stented with non-overlapping 3.5 x 12mm EES and BMS, and 24 h after receiving an intravenous injection of the inflammatory cathepsin protease activity imaging reporter Prosense VM110, rabbits underwent multimodal NIRF, IVUS, and angiographic imaging (*Figure 1*).

Intravascular NIRF imaging of cathepsin protease activity distinguished unstented plaques, plaque treated with BMS, and plaques treated with EES. In the unstented plaque zone, elevated NIRF signal was present thus indicating augmented inflammatory protease activity (*Figure 2*). IVUS provided anatomical detail (stent struts, atheroma, vessel morphology) that facilitated accurate anatomical co-registration with the NIRF signal (*Figure 2D*). In comparison to unstented and BMS-treated plaques, EES-treated plaques demonstrated reduced *in vivo* cysteine protease activity [TBR EES: 1.01 (0.92, 1.05) vs. BMS: 1.56 (1.32, 3.10) vs. unstented plaque: 2.29 (1.64, 5.10), (A) $P = 0.006$ (B) $P = 0.004$].

Ex vivo macroscopic FRI further mapped the 2D protease activity signal in stented and unstented aortic plaques (*Figure 3*). EES-treated plaques demonstrated respective 75 and 40% reductions in plaque inflammation compared with unstented plaques and BMS-stented plaques (TBR EES: 1.31 [1.18, 1.52] vs. BMS: 3.13 [1.6, 4.45] vs. unstented plaque: 5.24 [3.93, 5.99], $P = 0.003$; *Figure 4*). An edge-based relative increase in arterial wall inflammation was again noted suggested in EES-treated segments, but no statistical differences were evident when analysed across 3 mm stent intervals ($P = 0.94$ EES, $P = 0.81$ BMS).

EES-treated plaques demonstrate reduced macrophage and cathepsin B expression

Macrophages and inflammatory proteases drive plaque progression and complications. To assess whether EES reduced inflammation in the arterial wall, immunostaining and quantification of vessel wall macrophages via RAM-11 marker detection was performed in resin-embedded sections. Quantitative IHC (10–15 sections analysed per group, *Figure 5*) demonstrated that EES-treated plaques contained substantially fewer macrophages than BMS-treated plaques ($P < 0.05$) and unstented plaques ($P < 0.05$). EES further demonstrated significant reductions in macrophages in the neointima and media compared with plaque intima and media, and significant reductions in neointimal macrophages compared with BMS.

Consistent with an expected reduction in neointimal hyperplasia, EES-treated plaques showed reduced neointimal tissue area and a lower luminal stenosis compared with BMS-treated plaques: [median neointimal area (mm^2), BMS: 2.130 (1.816, 2.957) vs. EES 1.510 (1.130, 1.593), $P = 0.029$; % stenosis, BMS: 20.33 (17.34, 26.12) vs. EES: 13.93 (10.53, 15.57), $P = 0.029$; *Figure 5D–E*].

Owing to loss of antigen expression of cathepsin B in resin-embedded sections, one additional rabbit underwent immunohistochemical analyses on cryosections obtained from OCT-embedded stents. Consistent with analyses of resin-embedded sections, cryosections showed reduced RAM-11 macrophage expression in EES-treated plaques compared with BMS-treated plaques, or unstented plaques (*Figure 6*). Immunohistochemical cathepsin B expression

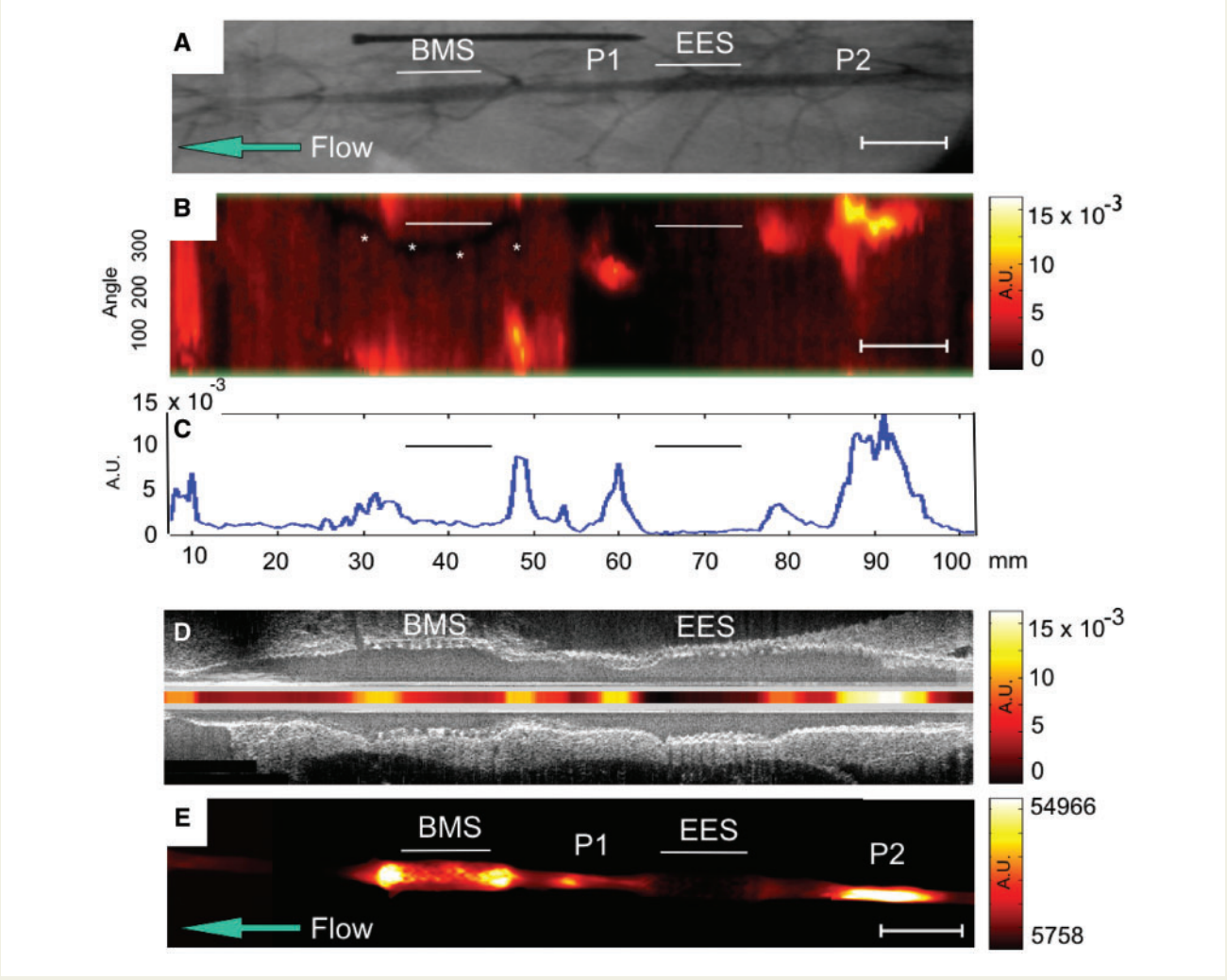

Figure 2 Multimodal *in vivo* and *ex vivo* imaging of inflammatory protease activity in BMS-, EES-treated, and unstented plaque zones in the abdominal aorta of a representative rabbit. (*A*) X-ray angiogram of the abdominal aorta. Straight lines show the position of the BMS and the EES. Areas of IVUS–visible plaque (P1 and P2 zones) are highlighted. The blue arrow designates direction of blood flow. (B) *In vivo* NIRF catheter pullback showing NIRF signal intensity in arbitrary fluorescence units. The *y*-axis represents the angular dimension (0°–360°). The *x*-axis represents the longitudinal/axial dimension in millimetres. The asterisk denotes a guidewire artefact. (*C*) 1D angle-averaged mean NIRF signal along the longitudinal axis. (*D*) Fusion of the aligned longitudinal IVUS and intravascular NIRF images. (*E*) *Ex vivo* FRI at 800 nm of the resected aorta. AU, arbitrary units; Scale bar, 10 mm.

paralleled macrophage expression and was reduced similarly in EES-treated plaques compared with BMS-treated plaques or unstented plaques. Morphological images demonstrated reduced neointimal hyperplasia in EES compared with BMS, consistent with the resin-embedded results.

Discussion

This investigation demonstrates that EES reduce macrophage-based inflammatory protease activity in atherosclerosis *in vivo*, as assessed by intravascular NIRF molecular imaging. Reductions in plaque protease activity were greater with EES compared with BMS, suggesting that everolimus induces significant *in vivo* anti-inflammatory effects in atheroma.

Via degradation of the extracellular matrix, cysteine proteases such as cathepsins, predominantly macrophage derived, contribute importantly to the progression and complications of atherosclerosis.[9,10] Using an activatable NIR fluorescence sensor in conjunction with an intravascular 2D NIRF imaging system, we found that EES reduced plaque cysteine protease activity *in vivo* compared with BMS and unstented plaque regions. Immunohistochemical studies demonstrated parallel reductions in plaque macrophages and cathepsin B expression in EES-treated atheroma compared with BMS-treated or unstented atheromata. Cathepsin B was utilized a model macrophage-derived cysteine protease, as it is a well-established reporter of Prosense VM110 activation in atherosclerosis.[7,8,12] These results extend the pivotal *ex vivo* study by Verheye *et al.*[4] that employed non-clinical everolimus coatings and polymers in conjunction with a stainless steel stent.

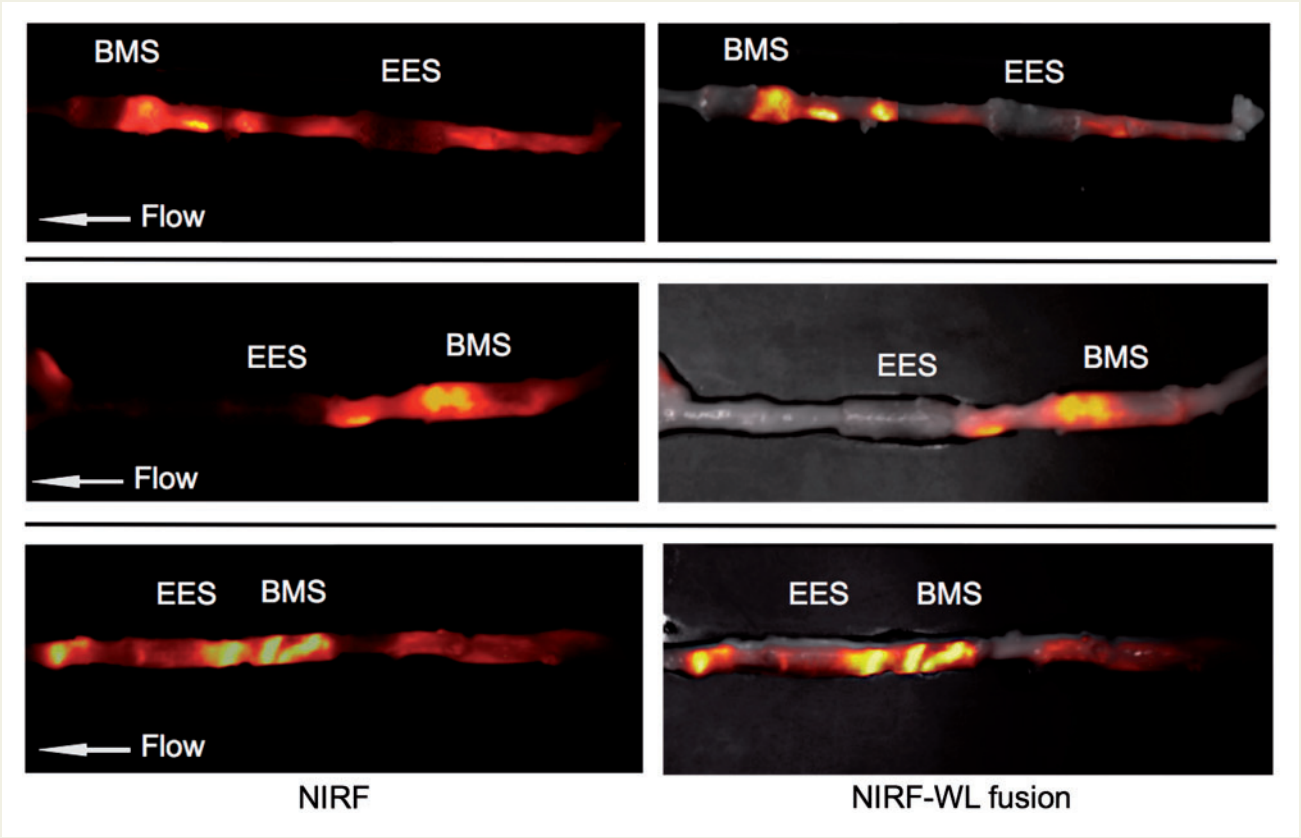

Figure 3 *Ex vivo* FRI analyses of plaque inflammatory cysteine protease activity in BMS-, EES-treated, and unstented plaque zones. (*A–C*) *Ex vivo* FRI alignments from three representative animals. All NIRF images were obtained with a one second exposure. Image windows optimized for individual images.

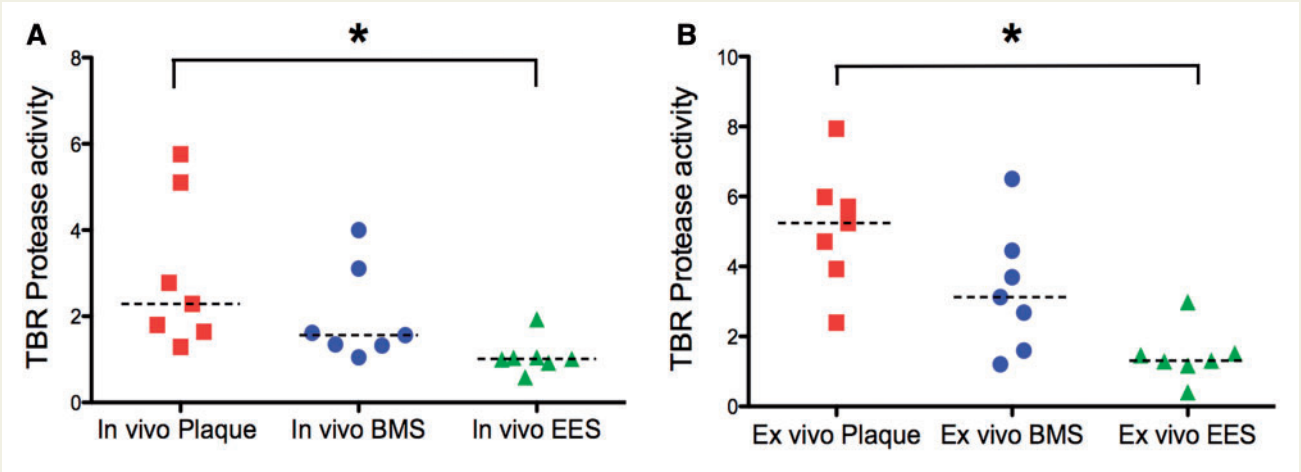

Figure 4 Quantification of the differences between (*A*) *in vivo* and (*B*) *ex vivo* NIRF inflammation signals among unstented plaque, BMS- and EES-treated atheroma ($n = 7$ rabbits). TBR, target-to-background. *$P < 0.05$.

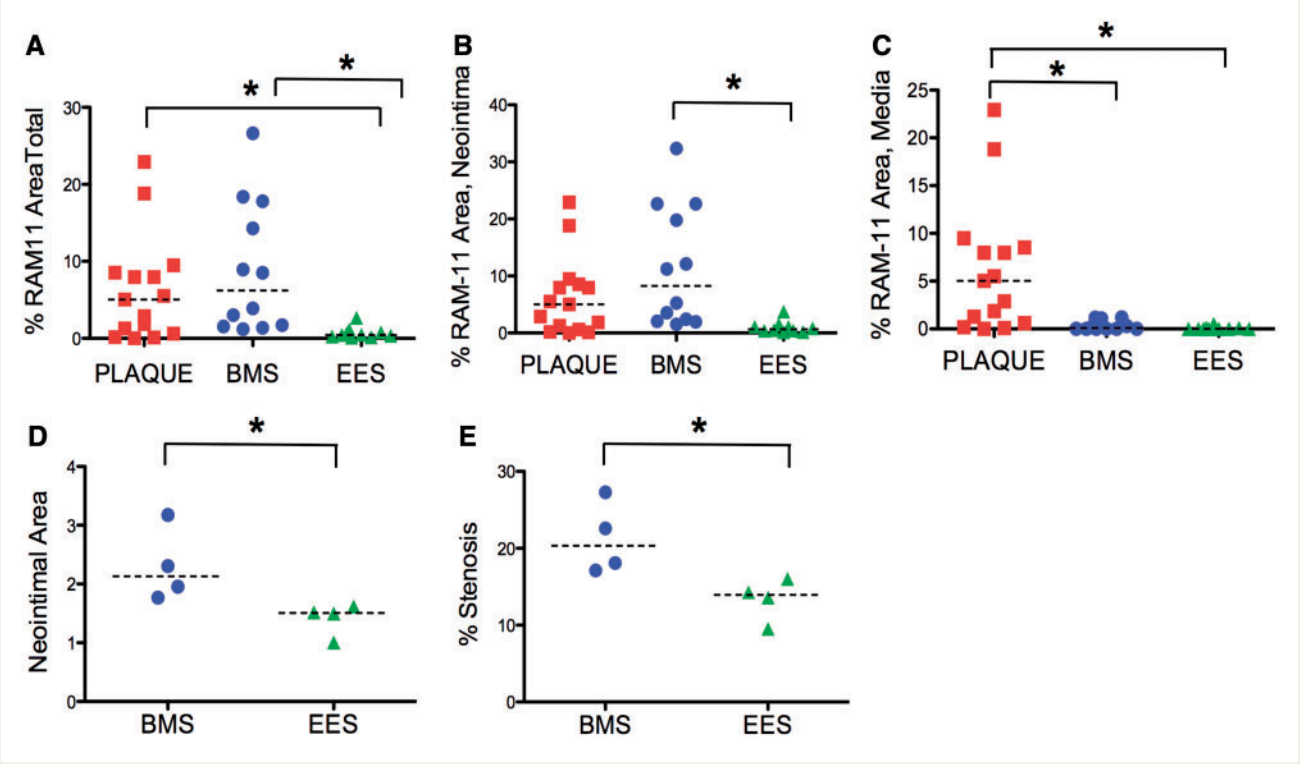

Figure 5 Histological assessment of macrophages and morphometry differences among resin-embedded plaque, BMS and EES segments. Macrophages were detected by RAM-11 immunohistochemical staining ($n = 37$ sections analysed). (*A*) Total macrophage area (neointima plus media, mm^2). (*B*) Neointimal macrophage area (mm^2). (*C*) Medial macrophage area (mm^2). (*D*) Neointimal area in BMS and EES (mm^2). (*E*) Luminal stenosis (%) in BMS and EES. $^*P < 0.05$.

Intravascular 2D NIRF molecular imaging is a new approach for assessing the anti-inflammatory effects of coronary stent-based therapeutics *in vivo*.[13,14] Intravascular NIRF signals from the arterial wall were readily detected through blood in real-time, in 3.5-mm diameter vessels. These results affirm that the NIR window is favourable for intravascular *in vivo* imaging, owing to substantially lower light attenuation and tissue autofluorescence compared with visible light range.[13,14] As NIR light does not penetrate metallic stent struts, the detected signal therefore reflects the protease activity within the stent cells (~80% of the arterial surface), and from tissue overlying stent struts. Intravascular NIRF imaging may therefore be well suited for assessing the *in vivo* biological effects of coronary stents with differing metal or biodegradable scaffolds, polymers, and biologics, could ultimately provide new insights into restenosis and stent thrombosis.

To image arterial inflammation *in vivo*, we employed the NIRF molecular imaging agent Prosense VM110, a reporter of cysteine protease activity in atherosclerosis and vascular injury.[7,8] The backbone of this NIRF imaging agent has safely completed Phase II clinical trials.[15] In addition to the potential for clinical use of VM110, the FDA has also approved NIRF imaging agents such as indocyanine green, widely utilized in retinal angiography and cardiac output studies, and which also shows promise for high-risk atherosclerosis detection.[16] Translationally, intracoronary NIRF catheters appear clinically viable, as several light-based catheter approaches [e.g. optical coherence tomography (OCT), near-infrared spectroscopy] are FDA-approved and have similar performance specifications (size, laser power) as the currently employed NIRF imaging system. A first-in-human study of NIR autofluorescence and OCT imaging in human coronary arteries[17] offers further support that intracoronary NIRF molecular imaging will be available in the near future.

While atherosclerosis is a systemic disease, acute myocardial infarction (AMI) arising from plaque disruption is a focal manifestation of coronary artery disease, and therefore local treatment of high-risk plaques might be effective.[18] As the location of the majority of plaques that cause AMI are amenable to percutaneous coronary intervention,[19] intracoronary stenting offers an intriguing approach for the stabilization of high-risk plaques in very high-risk patients.[3,18] Given the observed anti-inflammatory effects of EES compared with BMS, EES may offer an integrated structural and anti-inflammatory scaffold for treating inflamed, high-risk plaques. Indeed an everolimus-eluting scaffold is under investigation for treating high-risk coronary plaques (NCT02171065); whether this approach will reduce human plaque inflammation remains to be determined. As illustrated by the current results, as NIRF catheter and imaging agent technology becomes clinically available, it may be possible to understand the anti-inflammatory effects of DES and scaffolds on coronary plaques in patients.

Limitations of the study are present. While the sample size was relatively small, the *in vivo* and *ex vivo* data demonstrate that EES can significantly suppress plaque inflammation, and are consistent with

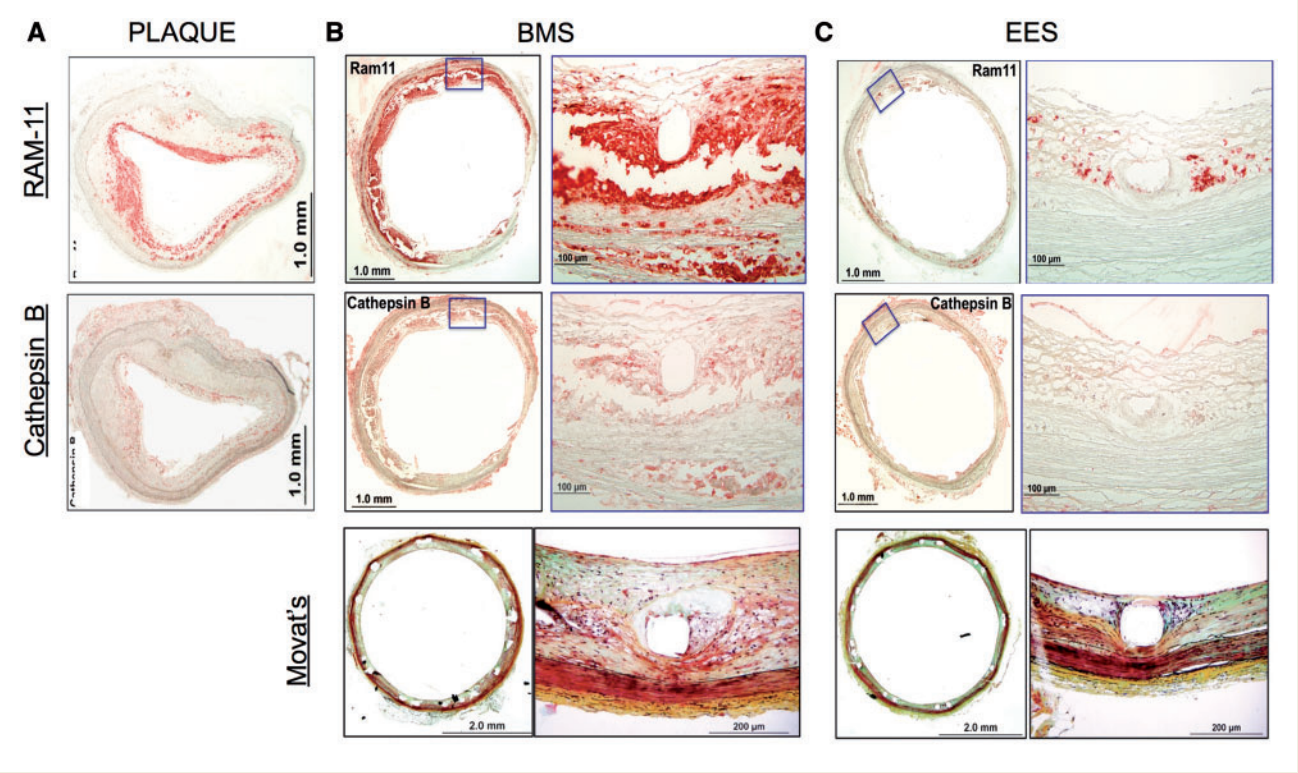

Figure 6 Immunohistochemical detection of cathepsin B and macrophages from cryosections of plaque, BMS and EES segments. (*A*) Low magnification (2×) images of cryosections from a plaque demonstrating abundant immunoreactive macrophage RAM-11 and cathepsin B. (*B*, *C*) Immunohistochemical macrophage and cathepsin B expression, and morphological image, of a (B) BMS-treated segment and (C) EES-treated segment. Inset magnification, ×20.

prior *ex vivo* data from Verheye *et al.*[4] NIRF signals are inversely weighted by distance to the arterial wall, an effect that is magnified in the presence of light-attenuating blood. To reduce the effects of surface weighting, inflammation TBRs were averaged over the entire 12 mm of stent length. Additional NIRF signal processing solutions include distance-based light attenuation correction,[20] which could be enabled *in vivo* with the development of single-integrated structural-NIRF catheters, e.g. IVUS/NIRF or OCT/NIRF catheters, which were not available at the time of this study. Polymer-only stents were not available during this study, and we focused on using clinically employed stents. Serial NIRF imaging was not performed in this study owing to concerns that signal from Prosense VM110 could persist from the first imaging timepoint and confound NIRF signal measurements at the final timepoint. Additional studies characterizing the washout kinetics of NIRF imaging agents will be an important focus for future studies that employ serial NIRF imaging.

In conclusion, EES locally suppress plaque inflammatory protease activity *in vivo* as assessed by translatable intravascular NIRF molecular imaging. These results further support EES as a local approach for plaque stabilization.

Conflict of interest: F.A.J.—Research grant and non-financial research support, Abbott Vascular, investigator-initiated sponsored research agreement; Consultant, Boston Scientific, Abbott Vascular. R.V.—Honoraria, Abbott Vascular, Terumo, Arsenal Medical, WL Gore, Biosensors, Medtronic CardioVascular, Lutonix; Speakers Bureau, Merck; Consultant, Medtronic CardioVascular, Abbott Vascular, Arsenal Medical, Neotract, WL Gore, Atrium Medical, GSK. A.S. and I.V.P.—Employees of Abbott Vascular.

Funding

National Institutes of Health grant R01 HL108229 and HL122388 (F.A.J.), Abbott Vascular (Investigator-initiated sponsored research agreement to F.A.J.), American Heart Association Scientist Development Grant #0830352N (F.A.J.), Howard Hughes Medical Institute Early Career Award (F.A.J.), European Community's Seventh Framework Programme (FP7/2007–2013 under grant agreement #235689 to A.R.), and the MGH William Schreyer Fellowship (M.A.C.) and Hassenfeld Scholar Award (F.A.J).

References

1. Libby P, Ridker PM, Hansson GK. Progress and challenges in translating the biology of atherosclerosis. *Nature* 2011;**473**:317–25.
2. Kaptoge S, Di Angelantonio E, Lowe G, Pepys MB, Thompson SG, Collins R *et al*. C-reactive protein concentration and risk of coronary heart disease, stroke, and mortality: an individual participant meta-analysis. *Lancet* 2010;**375**:132–40.
3. Wykrzykowska JJ, Diletti R, Gutierrez-Chico JL, van Geuns RJ, van der Giessen WJ, Ramcharitar S *et al*. Plaque sealing and passivation with a mechanical self-expanding low outward force nitinol vShield device for the treatment of IVUS and OCT-derived thin cap fibroatheromas (TCFAs) in native coronary arteries: report of the pilot study vShield Evaluated at Cardiac hospital in Rotterdam for Investigation and Treatment of TCFA (SECRITT). *EuroIntervention* 2012;**8**:945–54.

4. Verheye S, Martinet W, Kockx MM, Knaapen MW, Salu K, Timmermans JP *et al.* Selective clearance of macrophages in atherosclerotic plaques by autophagy. *J Am Coll Cardiol* 2007;**49**:706–15.
5. Van Dyck CJ, Hoymans VY, Bult H, Fransen E, Haine S, Bosmans JM *et al.* Resolute and Xience V polymer-based drug-eluting stents compared in an atherosclerotic rabbit double injury model. *Catheter Cardiovasc Interv* 2013;**81**:E259–68.
6. Zhao HQ, Nikanorov A, Virmani R, Schwartz LB. Inhibition of experimental neointimal hyperplasia and neoatherosclerosis by local, stent-mediated delivery of everolimus. *J Vasc Surg* 2012;**56**:1680–8.
7. Jaffer FA, Calfon MA, Rosenthal A, Mallas G, Razansky RN, Mauskapf A *et al.* Two-dimensional intravascular near-infrared fluorescence molecular imaging of inflammation in atherosclerosis and stent-induced vascular injury. *J Am Coll Cardiol* 2011;**57**:2516–26.
8. Jaffer FA, Vinegoni C, John MC, Aikawa E, Gold HK, Finn AV *et al.* Real-time catheter molecular sensing of inflammation in proteolytically active atherosclerosis. *Circulation* 2008;**118**:1802–9.
9. Liu J, Sukhova G, Sun J, Xu W, Libby P, Shi G. Lysosomal cysteine proteases in atherosclerosis. *Arterioscler Thromb Vasc Biol* 2004;**24**:1359–66.
10. Lutgens S, Cleutjens K, Daemen M, Heeneman S. Cathepsin cysteine proteases in cardiovascular disease. *FASEB J* 2007;**21**:3029–41.
11. Razansky RN, Rosenthal A, Mallas G, Razansky D, Jaffer FA, Ntziachristos V. Near-infrared fluorescence catheter system for two-dimensional intravascular imaging *in vivo*. *Opt Express* 2010;**18**:11372–81.
12. Chen J, Tung CH, Mahmood U, Ntziachristos V, Gyurko R, Fishman MC *et al. In vivo* imaging of proteolytic activity in atherosclerosis. *Circulation* 2002;**105**:2766–71.
13. Press MC, Jaffer FA. Molecular intravascular imaging approaches for atherosclerosis. *Curr Cardiovasc Imaging Rep* 2014;**7**:9293.
14. Mulder WJ, Jaffer FA, Fayad ZA, Nahrendorf M. Imaging and nanomedicine in inflammatory atherosclerosis. *Sci Transl Med* 2014;**6**:239sr1.
15. Callahan RJ, Bogdanov A Jr, Fischman AJ, Brady TJ, Weissleder R. Preclinical evaluation and phase I clinical trial of a 99mTc-labeled synthetic polymer used in blood pool imaging. *AJR Am J Roentgenol* 1998;**171**:137–43.
16. Vinegoni C, Botnaru I, Aikawa E, Calfon MA, Iwamoto Y, Folco EJ *et al.* Indocyanine green enables near-infrared fluorescence imaging of lipid-rich, inflamed atherosclerotic plaques. *Sci Transl Med* 2011;**3**:84ra45.
17. Ughi GJ, Wang H, Gerbaud E, Gardecki JA, Fard AM, Hamidi E *et al.* Clinical characterization of coronary atherosclerosis with dual-modality OCT and near-infrared autofluorescence imaging. *JACC Cardiovasc Imaging* 2016;**9**(11):1304–14.
18. Braunwald E. Epilogue: what do clinicians expect from imagers? *J Am Coll Cardiol* 2006;**47**(8 Suppl):C101–3.
19. Wang JC, Normand SL, Mauri L, Kuntz RE. Coronary artery spatial distribution of acute myocardial infarction occlusions. *Circulation* 2004;**110**:278–84.
20. Mallas G, Brooks DH, Rosenthal A, Nudelman RN, Mauskapf A, Jaffer FA *et al.* Improving quantification of intravascular fluorescence imaging using structural information. *Phys Med Biol* 2012;**57**:6395–406.